All-fiber spot-size transformer for efficient free-space optical interconnecting devices

Kyung-Rok Kim and Kyunghwan Oh

A new concatenated configuration of optical fibers is proposed to improve misalignment tolerance and working distance in a free-space optical interconnection. The structure is composed of three segments: a thermally expanded core fiber, a coreless silica fiber, and a claddingless graded-index fiber. A numerical analysis for the design of each fiber segment is performed completely, and the device characteristics are experimentally evaluated in terms of the tolerances for a 1-dB coupling-loss increment against longitudinal, transverse, and angular misalignments. © 2003 Optical Society of America

OCIS codes: 060.0060, 060.2310, 060.2340, 350.3950.

1. Introduction

The recent increase in the demand for optical fiber devices operating in free space, such as a microelectromechanical system (MEMS) switch, an in-line isolator, a pigtailed laser diode (LD), and an arrayed waveguide grating, requires advanced techniques for fiber interconnection. A reliable interconnecting technique requires a simple robust structure, a reliable fabrication process, and a compact size for mass production. Another important requirement in the fiber interconnection is improvement of the tolerances in misalignments such as longitudinal, transverse, and angular displacements. Owing to diffraction, the divergence of the beam is inversely proportional to the initial spot size, defined as the half-width at $1/e^2$ of the Gaussian intensity distribution, which sets a fundamental limit on the misalignment tolerances. To circumvent the rapid beam divergence from the optical fiber ends, a beam-expanding method has been established to connect fiber to fiber, fiber to LD, or fiber to integrated optics, where external lens media are conventionally used. In particular, quarter-pitch parabolic-index lenses have been used to construct micro-optic devices, wavelength division multiplexers/demultiplexers, a spot-size converter for LD-to-fiber coupling, and optical fiber switches.[1–3]

The lens elements, however, require precise alignment procedures, which results in a complicated optical design, a large form factor, environmental vulnerability, as well as expensive packaging. Therefore it is worthwhile to investigate an alternative approach to an all-fiber free-space interconnection technique that could obviate the lens media. Thermally expanded core (TEC) fiber has been attempted as one all-fiber solution, in which the spot size was enlarged by the diffusion of dopants in the core.[4–6] The core of the TEC fiber was expanded adiabatically in the longitudinal direction so that the insertion loss was negligible. Another all-fiber solution was use of graded-index (GRIN) multimode fibers (MMFs).[7–10] Because of the quadratic index profile, the GRIN MMF acts as a lens element when an appropriate length is spliced to a single-mode fiber (SMF), and the technique can provide several advantages over a conventional bulk lens media such as a common fiber/lens diameter, a stable fused fiber interface, and a small form factor.[7] Figure 1 schematically shows various fiber interconnecting techniques that use GRIN MMF. The input from the SMF excites modes in the GRIN MMF that propagate in an periodic optical path as shown in Fig. 1(a). When a GRIN fiber is cleaved at a quarter-pitch, the segment acts as a beam collimator as shown in Fig. 1(b). When the GRIN fiber segment exceeds the quarter-pitch, it functions as a focusing lens as in Fig. 1(c). If a coreless silica section is inserted between a GRIN fiber and a SMF, a larger beam expansion can be obtained as in Fig. 1(d).

In this paper we propose a new all-fiber free-space

The authors are with the Department of Information and Communications, Gwangju Institute of Science and Technology, 1 Oryong-dong, Puk-ku, Gwangju, 500-712, Korea. K. Oh's e-mail address is koh@kjist.ac.kr.

Received 6 March 2003.
0003-6935/03/316261-06$15.00/0

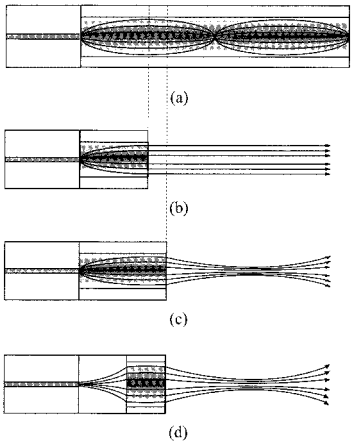

Fig. 1. Various schemes for beam expansion when GRIN MMF is used: (a) beam propagation in a GRIN fiber, (b) the beam collimation method, (c) the in-line focusing method, and (d) the expanding and in-line focusing method.

interconnecting technique by concatenating three fiber segments: a cladless GRIN MMF, a coreless silica fiber (CSF), and a TEC SMF. Figure 2 schematically illustrates the structure of the newly proposed fiber interconnector. The CSF was placed deliberately between the SMF and the cladless GRIN MMF to flexibly control the output spot size. One of the salient features of the proposed device is that we use a cladless GRIN MMF that can increase the output spot size within the entire fiber dimension of 125

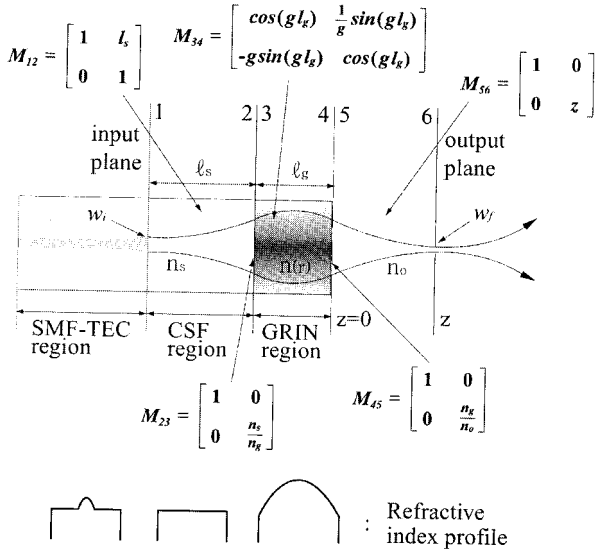

Fig. 2. Schematic view of the newly proposed fiber interconnector. When the core of the TEC fiber is expanded, coupling efficiency can be improved, and an increase in the aperture of the GRIN fiber makes it possible to expand the spot size more. The ray transformation matrix M_{ij} is given for propagation between planes i and j, where n_s, n_g, and n_o are the refractive indices of the CSF, the GRIN-MMF axis, and air, respectively; l_s and l_g are the lengths of the CSF and GRIN MMF, respectively; z is the distance from the endface of the fiber terminal; and g is a quadratic gradient constant of the GRIN MMF.

μm. Previous techniques in which GRIN-MMF were used for fiber-to-fiber interconnection and LD-to-fiber coupling had a fundamental limit imposed by the core diameter of the GRIN MMFs, which was 50–85 μm. The new configuration therefore could further increase both beam expansion efficiency and subsequent misalignment tolerance, a working distance from taking advantage of the 125-μm core.

Another notable feature of the proposed device is introduction of a TEC fiber, which could provide benefits for the LD-to-fiber couplings. Coupling a highly divergent optical beam through a GRIN MMF can cause the focused beam to blur from the higher-order aberration of the index distribution and refraction at the end of the fiber.[11,12] It could deteriorate optical-coupling efficiency that results in additional excess loss. The core of the TEC fiber can efficiently increase the acceptable area to reduce blurring-related excess loss. TEC fiber can also improve the fiber-length tolerance in CSF and GRIN-MMF segments, which is significant in practical manufacturing processes.

2. Numerical Analysis

In this section the optical beam propagation through the proposed device and free space are numerically analyzed to quantify the device parameters, such as the fiber-segment lengths, and their effects on focusing characteristics. To analyze the transformation of the optical field, we approximated with a Gaussian profile the modal field distribution at the input-fiber end, and the ray matrix transformation of the complex beam parameter after Kogelnik[13] and the square-law analysis of Kishimoto and Koyama[14] were utilized. Ray matrices in the proposed devices are listed in Fig. 2 for the input and output planes at the interfaces of the fiber segments and free space. The effective ABCD elements are obtained from

$$\begin{bmatrix} A & B \\ C & D \end{bmatrix} = M_{56}M_{45}M_{34}M_{23}M_{12}, \tag{1}$$

where M_{ij} is the matrix describing the transformation of the ray parameters between locations i and j. The input plane contains the endface of a fiber with a spot size of w_i. The output plane contains the final spot size w_f that formed after passing through a CSF, a GRIN fiber, and free space. Thus the spot size at the output plane is given by

$$w_f = w_i\left(\frac{n_s}{n_o}\frac{A^2 + a^2B^2}{AD - BC}\right)^{1/2}, \qquad a = \frac{\lambda}{\pi w_i^2 n_s}, \tag{2}$$

where λ is the wavelength and w_i and w_f are the initial and the final spot size, respectively. Note that the Gaussian-beam waist w is defined as the half-width at $1/e^2$ throughout this paper. The position of the beam waist z can be obtained with Eq. (3), which satisfies the beam-waist condition so that the beam radius of curvature R diverges to infinity.[7]

$$AC + a^2BD = 0. \tag{3}$$

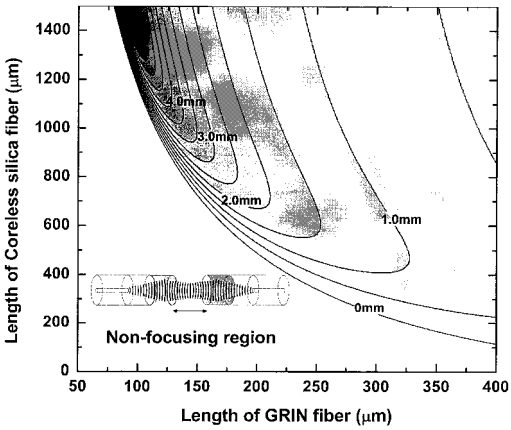

Fig. 3. Contour plot of the calculated working distance as a function of the length of the GRIN fiber and CSF.

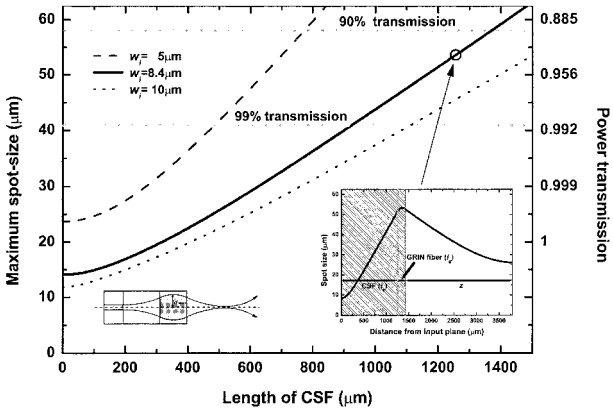

Fig. 5. Calculated maximum spot size in the proposed devices as a function of the length of the CSF.

The working distance, z doubled, and the spot size at the beam waist are obtained by solving Eqs. (2) and (3) for various fiber parameters. Note that the working distance is in fact the free-space length between two fiber terminals for maximum coupling. Figure 3 shows the contour plot of the calculated working distance $2z$ as a function of the CSF and GRIN-MMF segment lengths. The parameters used in the calculations are $g = 2.83\ \text{mm}^{-1}$, $\lambda = 1.55\ \mu\text{m}$, and $w_i = 8.4\ \mu\text{m}$. In Fig. 3 note that the working distance increases for a longer CSF and shorter GRIN fiber lengths. On the contrary the working distance decreases as the GRIN fiber length increases for a fixed CSF length. It is also observed that two values of the CSF length satisfy a single working distance for a certain length of GRIN fiber, which is attributed to diffraction in free space. Figure 4 shows the spot size at the beam waist as a function of the lengths of the CSF and the GRIN fiber. Note generally that the spot size increases for a longer CSF and shorter GRIN fiber lengths.

Using the results in Figs. 3 and 4, we can design the proposed device to have a prospective working distance and spot size at the beam waist, depending on applications, by adjusting the lengths of the CSF and the GRIN fiber. For example, a longer working distance is emphasized more in the MEMS and the application of in-line devices, while a tighter spot size is required more in fiber-to-waveguide mode-matching applications. Several restrictions exist, however, on the fiber-length parameters. In Fig. 4 the white region of the contour plot is designated as the nonfocusing region. In this region the fiber-length parameters in fact result in a diverging beam rather than a focused beam.

Another limitation is the CSF length. As the optical field propagates along the CSF, the spot size grows owing to diffraction but is limited by the CSF diameter, which is set at 125 μm in this study. If the CSF is too long, the optical field experiences the Fresnel reflection at the CSF and air boundary, resulting in excess loss. For example, the CSF length below 900 μm guarantees a power transmission greater than 99% theoretically when the initial spot size is 8.4 μm. The ratio of the power carried within an aperture of radius R in the transverse plane to the total power is derived by the integral of the optical intensity over a transverse plane and is summarized as

$$\text{Power transmission} = 1 - \exp\left(-2\,\frac{R^2}{w^2}\right), \quad (4)$$

where w is the Gaussian-beam spot size. Here the effect by reflection such as interference at the fiber–air interface is not considered.

Figure 5 represents the maximum allowed spot size and optical power transmission ratio in the proposed fiber interconnector as a function of the CSF length for various initial spot sizes. Note that the calculations are based on the common 125-μm diameter for the SMF, the CSF, and the GRIN MMF. A maximum allowed spot size smaller than 41 and 58 μm guarantees, respectively, 99% and 90% power transmission. The inset in Fig. 5 shows the ray trace of the proposed device as a specific example. The parameters are CSF length l_s, 1250 μm; the

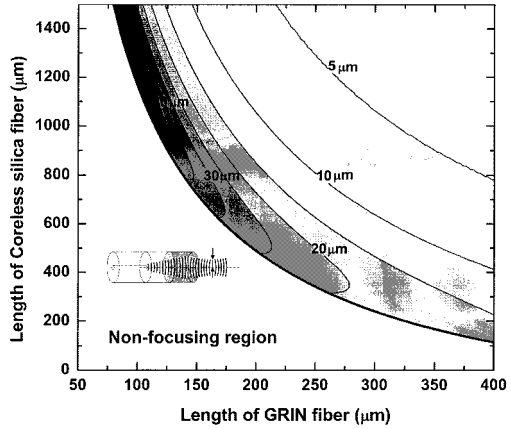

Fig. 4. Contour plot of the calculated spot size at the beam waist as a function of the length of the GRIN fiber and CSF.

Table 1. Calculated Optical Characteristics of Various GRIN Fibers as a Lens with 99% Transmission

Core diameter of GRIN fiber (μm)		50	85	125
Maximum working distance		400	1400	3100
Spot size at beam waist	Minimum	7.5	4.3	2.9
	Maximum	16	27	40
1-dB tolerance	Longitudinal	530	1510	3310
	Transverse	7.7	12.9	19.2

Note: $g = 2.83\ \text{mm}^{-1}$, $\lambda = 1.55\ \mu\text{m}$.

GRIN-MMF length l_g, 120 μm; and the input spot size after the SMF w_i, 8.4 μm. In this condition 94% power transmission is expected, as indicated by an open circle.

The cladless GRIN MMF proposed in this study shows several advantages compared with earlier results based on MMFs of smaller core. Table 1 shows a theoretical comparison of the characteristics of a GRIN fiber with different core diameters. At a power transmission ratio greater than 99%, the maximum working distance for the 125-μm core, the cladless MMF, increases by almost eightfold compared with the 50-μm-core GRIN fiber. The available range of spot size also increased by ~2.5 times. Owing to these improvements, 1-dB tolerance against longitudinal and transverse misalignment can be enhanced 6.2 and 2.5 times, respectively.

3. Fabrication Process

Before the actual fabrication of the device the design tolerance was analyzed against the error in the fiber-segment length. Figures 3 and 4 clearly demonstrate how the working distance and spot size are affected by the fiber-segment length. In a region of the long CSF and short GRIN-MMF lengths, for example, near the region around $l_s = 1250\ \mu\text{m}$ and $l_g = 120\ \mu\text{m}$, the spot size and the working distance vary by 22.6–30.9 and 4435–5414 μm, respectively, against an error of ±5 μm in the fiber-segment length. It is therefore found that precise control of fiber length within the micrometer range is required. In our fabrication process the reproducibility of the fiber-segment lengths was kept within ±4 μm, and the length could be measured with an accuracy of ±2 μm by an optical microscope.

A GRIN fiber preform of 22-mm diameter with a Ge-doped core of 13 mm was fabricated by modified chemical vapor deposition. To reduce the refractive-index dip at the center, the final core layer was etched with C_2F_6, which was followed by the tube collapse in a Ge-rich atmosphere. The perform was further annealed in a furnace at 1500 °C for 10 h to reduce the refractive-index irregularities in the core. Then the clad of the preform was completely etched away in a HF solution. The final preform was drawn into the optical fiber at a drawing speed of 15 m/min at a furnace temperature of 1950 °C. The waveguide structure of the cladless GRIN fiber is shown in Fig. 6 with $n = 1.471$, $\Delta = 1.5\%$, and $g = 2.83\ \text{mm}^{-1}$ at 1.55 μm.

The TEC fibers were fabricated by a flame-blush method. A Corning SMF-28 was heated by a microburner with a mixture of O_2 and C_3H_8 gases whose flow rates were 19 and 18 sccm, respectively. The burner traverse speed was 2 mm/s. To obtain core expansion, the traverse length was gradually decreased by 10 μm/step from an initial scanning length of 9 mm. A TEC fiber with a spot size of 8.4 μm was fabricated. The insertion loss was less than 0.01 dB.

The CSF was fabricated by drawing a silica glass rod. Using these fibers, we fabricated the proposed devices with the following steps. With an arc-discharge fiber splicer, a long CSF segment was first spliced to a TEC fiber, and then the other end was carefully cleaved at the desired distance. Then a long GRIN fiber segment was spliced to the CSF and cleaved at the desired distance. When these sequences were used, sample pairs consisting of $l_s = 1250\ \mu\text{m}$ and $l_g = 120\ \mu\text{m}$ and a TEC fiber with a 8.4-μm spot size were prepared.

4. Optical Coupling Losses in Free Space

It is theoretically known that an aperture size of πw_i is needed for 99% of the power transmission.[15] In recent applications such as MEMS, however, efforts to increase the working distance have been emphasized with a minimal increase in coupling loss. In this work we increased the spot size to larger than the theoretical limit for the lossless interconnection in order to facilitate a longer working distance and a

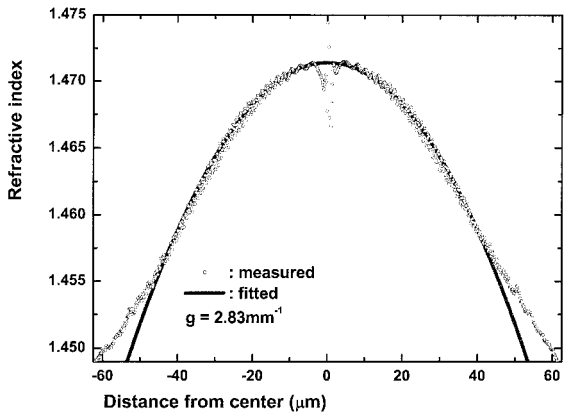

Fig. 6. Refractive-index distribution and fitted square-law profiles of the GRIN fiber used in the experiments: circles, refractive-index distribution; solid curve, fitted square-law profiles.

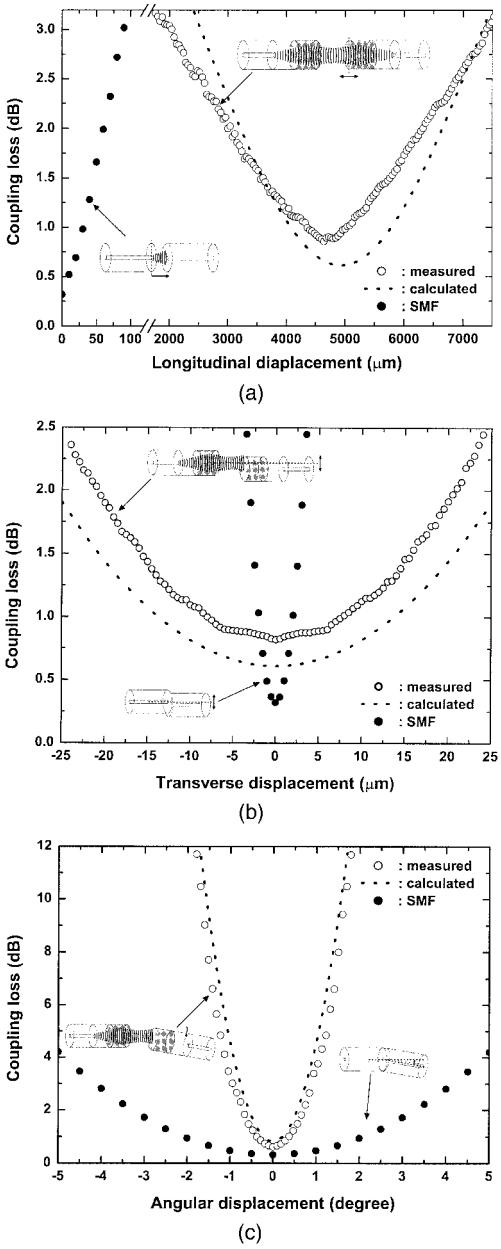

Fig. 7. Measured and calculated coupling losses as a function of (a) longitudinal, (b) transverse, and (c) angular displacements: solid circles, coupling loss of the normal SMF; open circles, proposed fiber interconnector; dotted curve, calculation.

high tolerance in longitudinal and transverse misalignments. In fact we could achieve a working distance of 4700 μm, an increment of 1.5-fold compared with the lossless spot size of πw_i, along with a slight increase in coupling loss to 0.29 dB by using the sample pairs mentioned in Section 3. Figure 7(a), 7(b), and 7(c) show the measured and the calculated coupling losses by longitudinal, transverse, and angular misalignment, respectively. The solid circles represent the SMF-to-SMF interconnection. The open circles represent the experimental measurements, and the dotted curves are theoretical predictions for a newly proposed device. Here a 1.55-μm LD was used as a light source. The insertion loss of the proposed pairs was less than 0.82 dB, which can be attributed to three different origins. The Fresenel reflection loss due to the absence of antireflection coating is ~0.32 dB. A spot size larger than the lossless value, mentioned in Section 3, is ~0.29 dB. The refractive-index irregularities of the GRIN fiber induced an additional excess loss of ~0.21 dB. The measured working distance was ~4.7 mm. For a loss increment of 1 dB the longitudinal and transverse tolerances of ±1540 and ±19.2 μm, respectively, were achieved. These values are 36.7 and 8.7 times higher than those for the conventional SMF, ±42 and 2.2 μm for longitudinal and transverse tolerances, respectively. The angular tolerance, however, significantly deteriorated compared with the SMF so that the tolerance angle was reduced to ±0.5° in the proposed device from ±2° in the SMF. Note that these results are comparable with or better than earlier techniques, and we could confirm that the proposed device could provide an all-fiber solution to enhance the efficiency of the free-space interconnection. The outstanding misalignment tolerance and long working distance of the newly proposed fiber interconnectors contribute to passive alignment fiber-optic devices so that compact, cost-effective, and robust packaging can be realized.

5. Conclusion

As an alternative to bulk lens elements in a fiber-based free-space interconnection, a new all-fiber configuration with a cascaded thermally expanded core single-mode fiber, a coreless silica fiber, and a cladless GRIN multimode fiber has been theoretically analyzed and experimentally demonstrated. The effects of the fiber-segment lengths were thoroughly analyzed for working distance, spot size, and power transmission. The advantages of cladless GRIN fiber have been numerically analyzed to confirm the enhancement of the optical parameter control. In the experiments the longitudinal and transverse displacement tolerances for a 1-dB coupling loss were ±1540 and ±19.2 μm, respectively, which are 36.7 and 8.7 times higher than those for the conventional SMF.

This work was supported in part by the Korea Science and Engineering Foundation through the Ultra-Fast Fiber-Optic Networks Research Center and by the Korean Ministry of Education through the BK21 project.

References

1. K. Kobayashi, R. Ishikawa, K. Minemura, and S. Sugimoto, "Micro-optic devices for fiber-optic communications," Fiber Integr. Opt. **2,** 1–7 (1979).
2. I. Kitano, H. Ueno, and M. Toyama, "Gradient-index lens for low-loss coupling of a laser diode to single-mode fiber," Appl. Opt. **25,** 3336–3339 (1986).
3. J. L. Jackel, S. Hackwood, and G. Beni, "Electrowetting optical switch," Appl. Phys. Lett. **40,** 4–6 (1982).

4. Y. Wang, T. Sato, J. Minowa, and H. Kataoka, "High-performance lensless in-line filters," Appl. Opt. **34,** 716–720 (1995).
5. T. Sato, J. Sun, R. Kasahara, and S. Kawakami, "Lens-free in-line optical isolators," Opt. Lett. **24,** 1337–1339 (1999).
6. K. Kato, I. Nishi, K. Yohino, and H. Hanafusa, "Optical coupling characteristics of laser diodes to thermally diffused expanded core fiber coupling using an aspheric lens," IEEE Photonics Technol. Lett. **5,** 469–470 (1991).
7. W. L. Emkey and C. A. Jack, "Analysis and evaluation of graded-index fiber lenses," J. Lightwave Technol. **LT-5,** 1156–1164 (1987).
8. P. Chanclou, M. Thual, J. Lostec, D. Pavy, M. Gadonna, and A. Poudoulec, "Collective micro-optics of fiber ribbon for optical interconnection devices," J. Lightwave Technol. **17,** 924–928 (1999).
9. K. Shiraishi, H. Ohnuki, N. Hiraguri, K. Matsumura, I. Ohishi, H. Morichi, and H. Kazami, "A lensed-fiber coupling scheme utilizing a graded-index fiber and hemispherically ended coreless fiber tip," J. Lightwave Technol. **15,** 356–363 (1997).
10. A. Ogura, S. Kuchiki, K. Shiraishi, K. Ohta, and I. Oishi, "Efficient coupling between laser diodes with a highly elliptic field and single-mode fibers by means of GIO fibers," IEEE Photonics Technol. Lett. **13,** 1191–1193 (2001).
11. K. Iga, "Theory for gradient-index imaging," Appl. Opt. **19,** 1039–1043 (1970).
12. K. Iga, "Evaluation and reduction of aberrations in distributed-index lens: review," Appl. Opt. **21,** 1024–1029 (1982).
13. H. W. Kogelnik, "On the propagation of Gaussian beams of light through lenslike media including those with a loss and gain variation," Appl. Opt. **4,** 1562–1569 (1965).
14. R. Kishimoto and M. Koyama, "Coupling characteristics between single-mode fiber and square-law medium," IEEE Trans. Microwave Theory Tech. **MTT-30,** 882–893 (1982).
15. B. E. A. Saleh and M. C. Teich, *Fundamentals of Photonics* (Wiley, New York, 1991), p. 85.